

We are IntechOpen, the world's leading publisher of Open Access books Built by scientists, for scientists

6,900

Open access books available

186,000

International authors and editors

200M

Downloads

Our authors are among the

154

Countries delivered to

TOP 1%

most cited scientists

12.2%

Contributors from top 500 universities



WEB OF SCIENCE™

Selection of our books indexed in the Book Citation Index
in Web of Science™ Core Collection (BKCI)

Interested in publishing with us?
Contact book.department@intechopen.com

Numbers displayed above are based on latest data collected.
For more information visit www.intechopen.com



Diffraction by a Rectangular Hole in a Thick Conducting Screen

Hirohide Serizawa

Abstract

The phenomenon of diffraction by a rectangular hole in a thick conducting screen is investigated for various structural parameters (aperture sizes, aspect ratios, and screen thicknesses) and some incident angles by making use of the exact solution based on the Kobayashi potential (KP) when an electromagnetic (EM) plane wave with any polarization is impinged on the aperture. Since the KP method yields an eigenfunction expansion of the present geometry, the solution satisfies the proper edge condition as well as all the boundary conditions, and therefore we can obtain highly accurate and fast-convergent results. Many numerical results, which are useful for scientists and engineers, are provided for various physical quantities, such as the far-field diffracted pattern, transmission coefficients (normalized transmitted power), and aperture electric field distributions, and by using these numerical results, we examine the convergent property of the KP solution and discuss the effect of the hole size and shape, screen thickness, and incident polarization on the transmission property of the rectangular hole.

Keywords: electromagnetic wave, exact solution, rectangular hole, thick screen, diffraction, transmission, aperture field

1. Introduction

A rectangular hole in a conducting screen with nonzero thickness is a fundamental structure and its diffraction property of an electromagnetic (EM) wave is of great importance in many fields of engineering and physics. For example, the knowledge of EM wave transmission through and radiation from the rectangular aperture with a finite thickness helps to design an aperture-type antenna like a slot antenna and to solve the problems of electromagnetic compatibility (EMC)/electromagnetic interference (EMI). The first theoretical work on this problem (three-dimensional problem) was made by Jin and Volakis by combining the finite element and the boundary integral methods [1]. From then, this problem has been solved by a variety of methods, such as the Fourier transform and mode-matching technique [2], a technique based on a perturbation method and modified Green's functions [3] and so on. In the field of physics, the extraordinary optical transmission (EOT) phenomena for subwavelength apertures have attracted considerable attention, and the study of the optical properties of holes in metallic films has become extremely active [4]. Garcia-Vidal et al. have applied the method based on the mode-expansion and mode-matching technique with some approximations to examine the transmission property of a single rectangular hole in a screen made of a perfect

electric conductor (PEC) [5] and of a real metal (with surface impedance) [6]. A similar modal method (but without any approximation in the formulation) was used by Brok and Urbach to calculate the transmission through holes [7]. Many methods have thus been used to solve the EM wave diffraction by a rectangular hole in a thick screen, but all the methods mentioned above do not consider the field singularity at aperture edges in the formulation (e.g., EM fields near the edge of a deep hole are considered to behave like those around the right-angled wedge). It is well known that the incorporation of the proper edge condition [8] into the field is effective in obtaining a highly accurate and faster convergent solution, and the method that can take into account the edge property is required to obtain the exact solution. The method of the Kobayashi potential (KP) [9] is a rigorous technique for solving mixed boundary value problems and has been successfully applied to many three-dimensional wave scattering and radiation problems to obtain exact solutions [10–14]. The KP method uses the discontinuous properties of the Weber-Schafheitlin (WS) integrals to satisfy a part of the boundary conditions, and, at this step, the required edge condition can be incorporated into the solution. Serizawa and Hongo applied the KP method to the problem of diffraction of an EM plane wave by a rectangular hole in a PEC screen with a finite thickness and derived the exact solution of the diffracted wave that satisfy the proper edge condition as well as all the boundary conditions [15]. By using the derived KP solution, the physical quantities such as the transmission coefficient, far diffracted fields, and power flow around the hole have been calculated for small and large apertures [16–18], but the numerical results for apertures greater than the half-wavelength in [16] contain errors because of the mistake in the calculation code of double infinite series.

In this chapter, using the KP solution, we provide many numerical results of various physical quantities useful for scientists and engineers, and we investigate the convergent property of the KP solution and the transmission property of the rectangular hole in the thick conducting screen for various structural parameters (aperture sizes, aspect ratios, and screen thicknesses) and some incident angles (all the numerical results in this chapter are newly calculated by using the improved calculation code that can give more accurate results than the previous code).

2. Formulation

Consider an EM plane wave diffracted by a $2a \times 2b$ size rectangular hole in an infinitely large conducting screen with a finite thickness d as shown in **Figure 1**. The screen is made of a PEC, and the center of the upper aperture is chosen as the origin O of the Cartesian coordinates (x, y, z) . The space is filled with an isotropic homogeneous medium with parameters (ϵ, μ) . Through this chapter, a harmonic time dependence $\exp(j\omega t)$ is assumed and omitted from the equations. The expression of the incident wave (the angles of incidence are θ_0 and ϕ_0) is given by

$$\mathbf{E}^{inc} = (E_1 \mathbf{i}_\phi + E_2 \mathbf{i}_\theta) \exp[jk\Phi^{inc}(\mathbf{r})] \quad (1)$$

$$\mathbf{H}^{inc} = Y(E_1 \mathbf{i}_\theta - E_2 \mathbf{i}_\phi) \exp[jk\Phi^{inc}(\mathbf{r})] \quad (2)$$

where $k = \omega\sqrt{\epsilon\mu}$, $Y = \sqrt{\epsilon/\mu}$, and

$$\mathbf{i}_\theta = \cos \theta_0 \cos \phi_0 \mathbf{i}_x + \cos \theta_0 \sin \phi_0 \mathbf{i}_y - \sin \theta_0 \mathbf{i}_z \quad (3)$$

$$\mathbf{i}_\phi = -\sin \phi_0 \mathbf{i}_x + \cos \phi_0 \mathbf{i}_y \quad (4)$$

$$\Phi^{inc}(\mathbf{r}) = x \sin \theta_0 \cos \phi_0 + y \sin \theta_0 \sin \phi_0 + z \cos \theta_0. \quad (5)$$

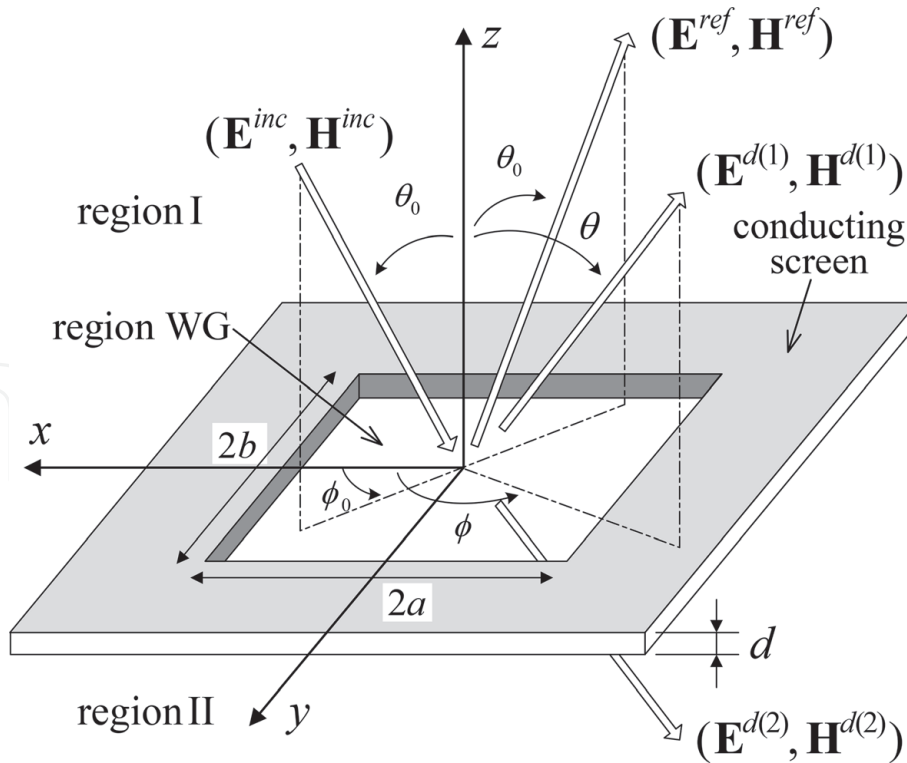


Figure 1. Plane wave diffraction by a rectangular hole in a perfectly conducting infinite screen with a finite thickness d . The hole size is $2a \times 2b$, and the center of the upper aperture is chosen as the origin of the Cartesian coordinates.

In **Figure 1**, \mathbf{E}^{ref} is the reflected wave when the plane $z = 0$ is occupied by an infinite conducting screen.

2.1 Field expression in each region

To solve the problem, we split the space into three regions I, II, and WG, denoting the upper and lower half-spaces, and waveguide region, respectively. Needless to say, $\mathbf{E}^{d(2)}$ is the transmitted wave.

The fields in region WG are represented by a linear combination of the TE- and TM-modes, and the axial components of the electric and magnetic vector potentials are given by

$$\begin{pmatrix} F_z^+ \\ F_z^- \end{pmatrix} = a\epsilon \sum_{m=0}^{\infty} \sum_{\substack{n=0 \\ (m,n) \neq (0,0)}}^{\infty} \begin{pmatrix} A_{mn}^{(E)} \exp(-jh_{mn}z_a) \\ B_{mn}^{(E)} \exp(jh_{mn}z_a) \end{pmatrix} \cos \frac{m\pi}{2}(\xi + 1) \cos \frac{n\pi}{2}(\eta + 1) \quad (6)$$

$$\begin{pmatrix} A_z^+ \\ A_z^- \end{pmatrix} = \frac{\kappa^2}{\omega} \sum_{m=1}^{\infty} \sum_{n=1}^{\infty} \begin{pmatrix} A_{mn}^{(M)} \exp(-jh_{mn}z_a) \\ B_{mn}^{(M)} \exp(jh_{mn}z_a) \end{pmatrix} \sin \frac{m\pi}{2}(\xi + 1) \sin \frac{n\pi}{2}(\eta + 1) \quad (7)$$

$$h_{mn} = \sqrt{\kappa^2 - (m\pi/2)^2 - p^2(n\pi/2)^2}, \quad \kappa = ka, \quad p = a/b (= 1/q) \quad (8)$$

where $\xi = x/a$, $\eta = y/b$, and $z_a = z/a$ are the normalized coordinates.

For the diffracted waves in the half-spaces, we use the x - and y -components of the electric vector potential \mathbf{F} (the use of the tangential components to the aperture is indispensable to incorporate the edge condition correctly), and they are given by Fourier spectral representations. The condition that the tangential electric field vanishes on the conducting screen can be satisfied by using the WS integrals [15], and we have

$$F_x^{d(i)} = (-1)^i a \epsilon \sum_{m=0}^{\infty} \sum_{n=0}^{\infty} \int_0^{\infty} \int_0^{\infty} \left\{ \Lambda_{2m}^{\sigma}(\alpha) \cos \alpha \xi \left[A_{mn}^{x(i)} \Lambda_{2n}^{\tau}(\beta) \cos \beta \eta \right. \right. \\ \left. \left. + B_{mn}^{x(i)} \Lambda_{2n+1}^{\tau}(\beta) \sin \beta \eta \right] + \Lambda_{2m+1}^{\sigma}(\alpha) \sin \alpha \xi \left[C_{mn}^{x(i)} \Lambda_{2n}^{\tau}(\beta) \cos \beta \eta \right. \right. \\ \left. \left. + D_{mn}^{x(i)} \Lambda_{2n+1}^{\tau}(\beta) \sin \beta \eta \right] \right\} \frac{\exp \left[(-1)^i \zeta(\alpha, \beta) z_a^{(i)} \right]}{\zeta(\alpha, \beta)} d\alpha d\beta \quad (9)$$

$$F_y^{d(i)} = (-1)^i a \epsilon \sum_{m=0}^{\infty} \sum_{n=0}^{\infty} \int_0^{\infty} \int_0^{\infty} \left\{ \Lambda_{2m}^{\tau}(\alpha) \cos \alpha \xi \left[A_{mn}^{y(i)} \Lambda_{2n}^{\sigma}(\beta) \cos \beta \eta \right. \right. \\ \left. \left. + B_{mn}^{y(i)} \Lambda_{2n+1}^{\sigma}(\beta) \sin \beta \eta \right] + \Lambda_{2m+1}^{\tau}(\alpha) \sin \alpha \xi \left[C_{mn}^{y(i)} \Lambda_{2n}^{\sigma}(\beta) \cos \beta \eta \right. \right. \\ \left. \left. + D_{mn}^{y(i)} \Lambda_{2n+1}^{\sigma}(\beta) \sin \beta \eta \right] \right\} \frac{\exp \left[(-1)^i \zeta(\alpha, \beta) z_a^{(i)} \right]}{\zeta(\alpha, \beta)} d\alpha d\beta \quad (10)$$

$$\zeta(\alpha, \beta) = \sqrt{\alpha^2 + p^2 \beta^2 - \kappa^2}, \quad z_a^{(1)} = z_a, \quad z_a^{(2)} = z_a + d_a, \quad d_a = d/a \quad (11)$$

where $\Lambda_{\ell}^{\nu}(x) = J_{\ell+\nu}(x)/x^{\nu}$ and $J_n(x)$ is the Bessel function of order n . The index i corresponds to the region number ($i = 1$ for region I and $i = 2$ for region II). The expressions of (9) and (10) are the Kobayashi potentials for the present problem. Parameters σ and τ are selected so as to incorporate the correct edge property into the electric field [8], and the correct values for the right-angled wedge, which are seemed to be valid for a deep hole, are $\sigma = 7/6$ and $\tau = 1/6$ ($= \sigma - 1$). $A_{mn}^{x(i)} \sim D_{mn}^{x(i)}$ and $A_{mn}^{y(i)} \sim D_{mn}^{y(i)}$ are determined from the remaining boundary conditions on the aperture.

2.2 Matrix equation

We enforce the remaining boundary conditions that the tangential EM fields are continuous on the aperture and the resultant equations are projected into functional spaces of trigonometric functions and Gegenbauer polynomials by using their orthogonality (for details, see [15]). After some lengthy analysis, we have matrix equations for the expansion coefficients:

$$\begin{bmatrix} K_{Amnst}^{(u,v)} + S_{Amnst}^{\pm(u,v)} & (-1)^{u+v} p \left\{ G_{Amnst}^{(u,v)} + T_{Amnst}^{\pm(u,v)} \right\} \\ (-1)^{u+v} q \left\{ G_{Bmnst}^{(\bar{u},\bar{v})} + T_{Bmnst}^{\pm(\bar{u},\bar{v})} \right\} & K_{Bmnst}^{(\bar{u},\bar{v})} + S_{Bmnst}^{\pm(\bar{u},\bar{v})} \end{bmatrix} \begin{bmatrix} X_{mn}^{\pm(u,v)} \\ Y_{mn}^{\pm(\bar{u},\bar{v})} \end{bmatrix} \\ = 2j \begin{bmatrix} j^{u+v} P_x \Lambda_{2s+u}^{\tau'}(\kappa_a) \Lambda_{2t+v}^{\sigma'}(\kappa_b) \\ j^{\bar{u}+\bar{v}} q^2 P_y \Lambda_{2s+\bar{u}}^{\sigma'}(\kappa_a) \Lambda_{2t+\bar{v}}^{\tau'}(\kappa_b) \end{bmatrix}, \quad \begin{cases} s = 0, 1, 2, \dots \\ t = 0, 1, 2, \dots \end{cases} \\ (u, v) = (0, 0), (0, 1), (1, 0), (1, 1), \quad \bar{u} = 1 - u, \quad \bar{v} = 1 - v. \quad (13)$$

Here, $X_{mn}^{\pm(u,v)}$, $Y_{mn}^{\pm(u,v)}$, P_x , P_y , κ_a , and κ_b are defined as follows:

$$X_{mn}^{\pm(u,v)} = X_{mn}^{(1)(u,v)} \pm X_{mn}^{(2)(u,v)}, \quad Y_{mn}^{\pm(u,v)} = Y_{mn}^{(1)(u,v)} \pm Y_{mn}^{(2)(u,v)} \quad (14)$$

$$X_{mn}^{(i)(0,0)} = A_{mn}^{x(i)}, \quad X_{mn}^{(i)(0,1)} = B_{mn}^{x(i)}, \quad X_{mn}^{(i)(1,0)} = C_{mn}^{x(i)}, \quad X_{mn}^{(i)(1,1)} = D_{mn}^{x(i)} \quad (15)$$

$$Y_{mn}^{(i)(0,0)} = A_{mn}^{y(i)}, \quad Y_{mn}^{(i)(0,1)} = B_{mn}^{y(i)}, \quad Y_{mn}^{(i)(1,0)} = C_{mn}^{y(i)}, \quad Y_{mn}^{(i)(1,1)} = D_{mn}^{y(i)} \quad (16)$$

$$P_x = \kappa(E_1 \cos \theta_0 \cos \phi_0 + E_2 \sin \phi_0), \quad \kappa_a = \kappa \sin \theta_0 \cos \phi_0 \quad (17)$$

$$P_y = \kappa(E_1 \cos \theta_0 \sin \phi_0 - E_2 \cos \phi_0), \quad \kappa_b = q\kappa \sin \theta_0 \sin \phi_0. \quad (18)$$

In (12), $K_{A,B}$ and $G_{A,B}$ are the double infinite integrals of four Bessel functions, and they are given by

$$K_{Amnst}^{(u,v)} = \int_0^\infty \int_0^\infty \frac{\kappa^2 - \alpha^2}{\zeta(\alpha, \beta)} \Lambda_{2m+u}^\sigma(\alpha) \Lambda_{2s+u}^{\tau'}(\alpha) \Lambda_{2n+v}^\tau(\beta) \Lambda_{2t+v}^{\sigma'}(\beta) d\alpha d\beta \quad (19)$$

$$K_{Bmnst}^{(u,v)} = \int_0^\infty \int_0^\infty \frac{q^2 \kappa^2 - \beta^2}{\zeta(\alpha, \beta)} \Lambda_{2m+u}^\tau(\alpha) \Lambda_{2s+u}^{\sigma'}(\alpha) \Lambda_{2n+v}^\sigma(\beta) \Lambda_{2t+v}^{\tau'}(\beta) d\alpha d\beta \quad (20)$$

$$G_{Amnst}^{(u,v)} = \int_0^\infty \int_0^\infty \frac{\alpha\beta}{\zeta(\alpha, \beta)} \Lambda_{2m+1-u}^\tau(\alpha) \Lambda_{2s+u}^{\tau'}(\alpha) \Lambda_{2n+1-v}^\sigma(\beta) \Lambda_{2t+v}^{\sigma'}(\beta) d\alpha d\beta \quad (21)$$

$$G_{Bmnst}^{(u,v)} = \int_0^\infty \int_0^\infty \frac{\alpha\beta}{\zeta(\alpha, \beta)} \Lambda_{2m+1-u}^\sigma(\alpha) \Lambda_{2s+u}^{\sigma'}(\alpha) \Lambda_{2n+1-v}^\tau(\beta) \Lambda_{2t+v}^{\tau'}(\beta) d\alpha d\beta \quad (22)$$

and $S_{A,B}$ and $T_{A,B}$ are the double infinite series of four Bessel functions and they are given by

$$S_{Amnst}^{\pm(u,v)} = \pi^2 \sum_{m'=0}^\infty \sum_{n'=0}^\infty \frac{\Gamma_{2m'+1+u, 2n'+v}^\pm}{1 + \delta_{0, 2n'+v}} \left[\kappa^2 - \left(\frac{2m'+1+u}{2} \pi \right)^2 \right] \Lambda_{2m+u}^\sigma \left(\frac{2m'+1+u}{2} \pi \right) \\ \times \Lambda_{2s+u}^{\tau'} \left(\frac{2m'+1+u}{2} \pi \right) \Lambda_{2n+v}^\tau \left(\frac{2n'+v}{2} \pi \right) \Lambda_{2t+v}^{\sigma'} \left(\frac{2n'+v}{2} \pi \right) \quad (23)$$

$$S_{Bmnst}^{\pm(u,v)} = \pi^2 \sum_{m'=0}^\infty \sum_{n'=0}^\infty \frac{\Gamma_{2m'+u, 2n'+1+v}^\pm}{1 + \delta_{0, 2m'+u}} \left[q^2 \kappa^2 - \left(\frac{2n'+1+v}{2} \pi \right)^2 \right] \Lambda_{2m+u}^\tau \left(\frac{2m'+u}{2} \pi \right) \\ \times \Lambda_{2s+u}^{\sigma'} \left(\frac{2m'+u}{2} \pi \right) \Lambda_{2n+v}^\sigma \left(\frac{2n'+1+v}{2} \pi \right) \Lambda_{2t+v}^{\tau'} \left(\frac{2n'+1+v}{2} \pi \right) \quad (24)$$

$$T_{Amnst}^{\pm(u,v)} = \pi^2 \sum_{m'=0}^\infty \sum_{n'=0}^\infty \Gamma_{2m'+1+u, 2n'+v}^\pm \left(\frac{2m'+1+u}{2} \pi \right) \left(\frac{2n'+v}{2} \pi \right) \Lambda_{2m+1-u}^\tau \left(\frac{2m'+1+u}{2} \pi \right) \\ \times \Lambda_{2s+u}^{\tau'} \left(\frac{2m'+1+u}{2} \pi \right) \Lambda_{2n+1-v}^\sigma \left(\frac{2n'+v}{2} \pi \right) \Lambda_{2t+v}^{\sigma'} \left(\frac{2n'+v}{2} \pi \right) \quad (25)$$

$$T_{Bmnst}^{\pm(u,v)} = \pi^2 \sum_{m'=0}^\infty \sum_{n'=0}^\infty \Gamma_{2m'+u, 2n'+1+v}^\pm \left(\frac{2m'+u}{2} \pi \right) \left(\frac{2n'+1+v}{2} \pi \right) \Lambda_{2m+1-u}^\sigma \left(\frac{2m'+u}{2} \pi \right) \\ \times \Lambda_{2s+u}^{\sigma'} \left(\frac{2m'+u}{2} \pi \right) \Lambda_{2n+1-v}^\tau \left(\frac{2n'+1+v}{2} \pi \right) \Lambda_{2t+v}^{\tau'} \left(\frac{2n'+1+v}{2} \pi \right) \quad (26)$$

where δ_{mn} is the Kronecker delta and

$$\Gamma_{mn}^\pm = \frac{1}{\gamma_{mn}} \frac{1 \mp \exp(-\gamma_{mn} d_a)}{1 \pm \exp(-\gamma_{mn} d_a)}, \quad \gamma_{mn} = \sqrt{\left(\frac{m\pi}{2} \right)^2 + p^2 \left(\frac{n\pi}{2} \right)^2 - \kappa^2} = jh_{mn}. \quad (27)$$

In Eqs. (19)–(26), parameters σ' and τ' are determined by considering the edge property of the magnetic field [8]. When the hole is deep, we can use the edge condition of the right-angled wedge, and for this case the values of $\sigma' = -1/6$ ($= -\tau$) and $\tau' = 5/6$ ($= \sigma' + 1$) can be selected.

2.3 Physical quantities

The expression of the far-field is obtained by applying the stationary phase method to (9) and (10), and we have

$$F_x^{d(i)} = (-1)^i \frac{\pi q a^2 \epsilon}{2} \frac{\exp(-jkr)}{r} \sum_{m=0}^{\infty} \sum_{n=0}^{\infty} \left\{ \Lambda_{2m}^{\sigma}(\kappa_x) \left[A_{mn}^{x(i)} \Lambda_{2n}^{\tau}(\kappa_y) + j B_{mn}^{x(i)} \right. \right. \quad (28)$$

$$\left. \times \Lambda_{2n+1}^{\tau}(\kappa_y) \right] + \Lambda_{2m+1}^{\sigma}(\kappa_x) \left[j C_{mn}^{x(i)} \Lambda_{2n}^{\tau}(\kappa_y) - D_{mn}^{x(i)} \Lambda_{2n+1}^{\tau}(\kappa_y) \right] \Big\} \\ F_y^{d(i)} = (-1)^i \frac{\pi q a^2 \epsilon}{2} \frac{\exp(-jkr)}{r} \sum_{m=0}^{\infty} \sum_{n=0}^{\infty} \left\{ \Lambda_{2m}^{\tau}(\kappa_x) \left[A_{mn}^{y(i)} \Lambda_{2n}^{\sigma}(\kappa_y) + j B_{mn}^{y(i)} \right. \right. \quad (29)$$

$$\left. \times \Lambda_{2n+1}^{\sigma}(\kappa_y) \right] + \Lambda_{2m+1}^{\tau}(\kappa_x) \left[j C_{mn}^{y(i)} \Lambda_{2n}^{\sigma}(\kappa_y) - D_{mn}^{y(i)} \Lambda_{2n+1}^{\sigma}(\kappa_y) \right] \Big\} \\ \kappa_x = \kappa \sin \theta \cos \phi, \quad \kappa_y = q \kappa \sin \theta \sin \phi. \quad (30)$$

In the above expressions, θ and ϕ are the spherical coordinate angles (the angles of diffraction) shown in **Figure 1**, and r is the distance from the center point of each aperture to the observation point, that is, $r = \sqrt{x^2 + y^2 + z^2}$ for region I and $r = \sqrt{x^2 + y^2 + (z + d)^2}$ for region II (the origin of the spherical coordinate system for region II is selected at the center of the lower aperture). Far electromagnetic fields are obtained from $\mathbf{E} = -\epsilon^{-1} \nabla \times \mathbf{F}$ and $\mathbf{H} = Y \mathbf{i}_r \times \mathbf{E}$ (\mathbf{i}_r is a unit vector of a radial direction). The transmission coefficient T is defined by the ratio of the total radiated power W_T into the $z < -d$ dark space to the power of the incident plane wave W_i on the aperture; $T = W_T/W_i$. W_T can be obtained by integrating the radiated power over the lower hemisphere, and we use the Gauss-Legendre quadrature in practical computation. W_i is analytically calculated, and the result is $W_i = 4abY \cos \theta_0$ for $|\mathbf{E}^{inc}| = 1$. For oblique incidence, $T \cos \theta_0$, which is the same as the transmission coefficient normalized by the normal incident power $W_i(\theta_0 = 0)$, is useful to evaluate the actual transmitted power into region II.

The expression of the aperture electric field is obtained by differentiating (9) and (10) with respect to z , and the resultant expression is given by

$$E_x^{d(i)} = \frac{\Gamma(\sigma)\Gamma(\tau)}{2^{2-(\sigma+\tau)}} (1-\xi^2)^{\tau-\frac{1}{2}} (1-\eta^2)^{\sigma-\frac{1}{2}} \sum_{m=0}^{\infty} \sum_{n=0}^{\infty} (-1)^{m+n} \left\{ \frac{\Gamma(2m+1)}{\Gamma(2m+2\tau)} C_{2m}^{(\tau)}(\xi) \right. \\ \times \left[A_{mn}^{y(i)} \frac{\Gamma(2n+1)}{\Gamma(2n+2\sigma)} C_{2n}^{(\sigma)}(\eta) + B_{mn}^{y(i)} \frac{\Gamma(2n+2)}{\Gamma(2n+2\sigma+1)} C_{2n+1}^{(\sigma)}(\eta) \right] + \frac{\Gamma(2m+2)}{\Gamma(2m+2\tau+1)} \\ \times C_{2m+1}^{(\tau)}(\xi) \left[C_{mn}^{y(i)} \frac{\Gamma(2n+1)}{\Gamma(2n+2\sigma)} C_{2n}^{(\sigma)}(\eta) + D_{mn}^{y(i)} \frac{\Gamma(2n+2)}{\Gamma(2n+2\sigma+1)} C_{2n+1}^{(\sigma)}(\eta) \right] \Big\} \quad (31)$$

$$E_y^{d(i)} = -\frac{\Gamma(\sigma)\Gamma(\tau)}{2^{2-(\sigma+\tau)}} (1-\xi^2)^{\sigma-\frac{1}{2}} (1-\eta^2)^{\tau-\frac{1}{2}} \sum_{m=0}^{\infty} \sum_{n=0}^{\infty} (-1)^{m+n} \left\{ \frac{\Gamma(2m+1)}{\Gamma(2m+2\sigma)} C_{2m}^{(\sigma)}(\xi) \right. \\ \times \left[A_{mn}^{x(i)} \frac{\Gamma(2n+1)}{\Gamma(2n+2\tau)} C_{2n}^{(\tau)}(\eta) + B_{mn}^{x(i)} \frac{\Gamma(2n+2)}{\Gamma(2n+2\tau+1)} C_{2n+1}^{(\tau)}(\eta) \right] + \frac{\Gamma(2m+2)}{\Gamma(2m+2\sigma+1)} \\ \times C_{2m+1}^{(\sigma)}(\xi) \left[C_{mn}^{x(i)} \frac{\Gamma(2n+1)}{\Gamma(2n+2\tau)} C_{2n}^{(\tau)}(\eta) + D_{mn}^{x(i)} \frac{\Gamma(2n+2)}{\Gamma(2n+2\tau+1)} C_{2n+1}^{(\tau)}(\eta) \right] \Big\} \quad (32)$$

where $C_{\ell}^{(a)}(x)$ are the Gegenbauer polynomials and $\Gamma(x)$ is the gamma function.

3. Numerical results and discussion

To obtain the numerical results for the physical quantities of interest, the matrix Eq. (12) must be solved. The matrix elements consist of double infinite integrals and double infinite series that converge rather slowly, and we can compute them with the desired accuracy by applying the Hongo method [10]. For the double infinite integrals, the full range of integration that is equal to the first quadrant of the $(\alpha, p\beta)$ space is divided into several subdomains. The infinite integrals over the subdomains outside a very large radius are transformed into more simple forms by applying asymptotic expansions of the Bessel functions (the integrands of the infinite integrals are represented by some elementary functions), and the infinite integrals of the elementary functions are analytically carried out. The finite integrals of the Bessel functions are numerically performed by applying the Gauss-Legendre quadrature scheme (examples of the treatment are shown in [10–12]). For the double infinite series, the asymptotic expansions are applied to the summands (details are discussed in [13–15]). Once the expansion coefficients are determined by solving the matrix equations, we can readily obtain the physical quantities from their concise expressions derived in the previous section. Unless otherwise noted, the edge condition of the right-angled wedge ($\sigma = 7/6$, $\tau = 1/6$, $\sigma' = -1/6$, and $\tau' = 5/6$) is used, and $|\mathbf{E}^{inc}| = 1$ is selected in all of the following calculations. In practical computation, the matrix size is truncated to $2n_k^2 \times 2n_k^2$, where $n_k - 1$ is the maximum value of indices m, n, s , and t in (12). By changing the value of n_k , we can numerically verify the convergence of the solution.

3.1 Convergence of the KP solution

We first calculated the transmission coefficient for various aperture sizes, aspect ratios, screen thicknesses, and incident angles. **Figure 2** shows examples of the transmission coefficient T as a function of the n_k value for square holes of $2a = \lambda/2$ ($ka = \pi/2$), $2a = \lambda$ ($ka = \pi$), and $2a = 3\lambda$ ($ka = 3\pi$) (λ is the wavelength) at $\theta_0 = 0$, 45 degrees ($\phi_0 = 0$). The subscripts E and H denote the E-polarization ($E_1 = 1$,

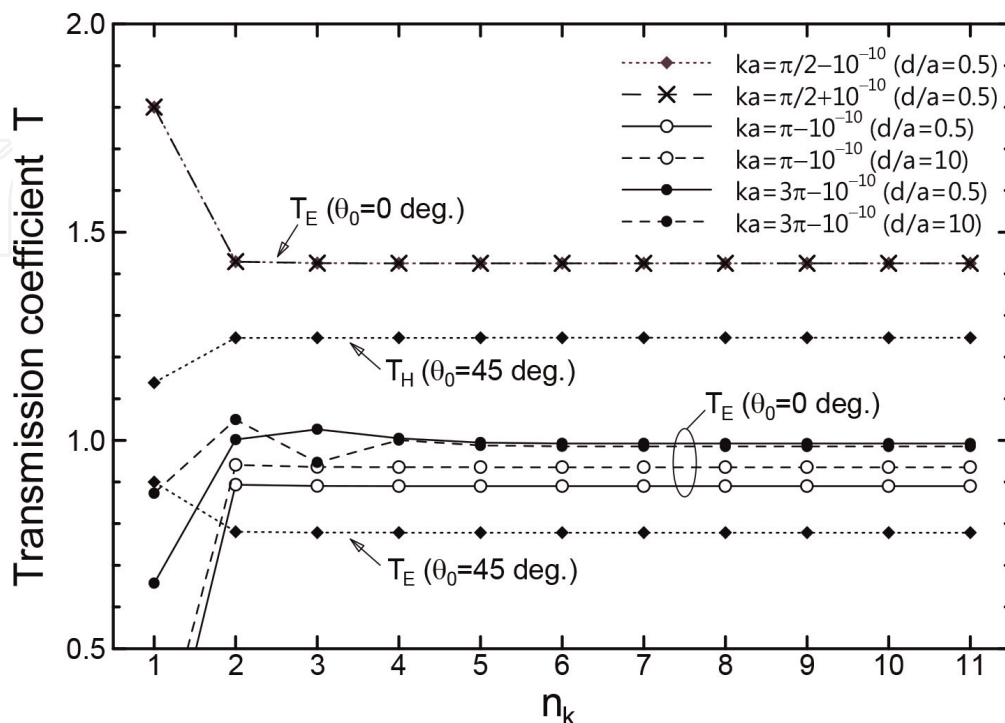


Figure 2. Convergence of T_E and T_H for square apertures of $2a = \lambda/2$, λ , and 3λ ($ka = \pi/2$, π , and 3π) at $\theta_0 = 0^\circ$, 45° , and $\phi_0 = 0^\circ$.

$E_2 = 0$) and H-polarization ($E_1 = 0, E_2 = 1$), respectively. For the normal incidence on the square hole, T_H is the same as T_E . From the figure, we see that the convergence is very rapid, and, for example, the results of $d/a = 0.5$ at $\theta_0 = \phi_0 = 0$ degrees have fully converged to four decimal places when $n_k = 4$ for $ka = \pi/2 - 10^{-10}$, $n_k = 5$ for $ka = \pi - 10^{-10}$, and $n_k = 7$ for $ka = 3\pi - 10^{-10}$. By the way, the summands of the series of (23)-(26) have singular points at $\gamma_{mn} = 0$ that arise for $ka = \ell\pi/2$ ($2a = \ell\lambda/2$), ($\ell = 1, 2, 3, \dots$). We can remove this singularity appropriately in the numerical calculation, but we here avoided the singularity by slightly shifting the ka value by $\pm 10^{-10}$. The results for $ka = \pi/2 \pm 10^{-10}$ have completely agreed for eight decimal places, and similar situations had held for other aperture sizes related with the singular points. Thus, this treatment is also applied for calculating the other physical quantities.

The convergent property of the KP solution was also examined for other physical quantities. **Figures 3–5** show the far-field patterns of three kinds of screen thicknesses for various sizes of square apertures ($ka = \pi/2 - 10^{-10}$ (small), $2\pi - 10^{-10}$, and $5\pi - 10^{-10}$ (very large)) at the normal incidence. The patterns are computed with $P(\theta) = \lim_{r \rightarrow \infty} 4\pi r^2 |\mathbf{E}^{d(i)}|^2 / |\mathbf{E}^{inc}|^2$, and they are given for different n_k values. It can be seen from the figure that the plotted lines converge with relatively small value of n_k ($n_k = 2$ for $ka = \pi/2 - 10^{-10}$, $n_k = 4$ for $ka = 2\pi - 10^{-10}$, and $n_k = 9$ for $ka = 5\pi - 10^{-10}$). **Figures 6 and 7** show the amplitude distributions of aperture electric field E_y (the co-polarized component) for thin ($d/a = 0.001$) and thick ($d/a = 0.5$) screen cases, respectively. The rate of convergence of thick case is very fast but is very slow for thin case, and we think this is caused by using the edge condition of the right-angled wedge (in spite of the use of the right-angled wedge condition, the convergence of the far-field is very fast as shown in **Figure 3**. This is due to the fact that the far-field has a stationary nature, that is, it changes little for small changes in field distribution). We also calculate E_y for thin screen case by applying the edge condition of zero-thickness plate, and the results corresponding to **Figure 6** are given in **Figure 8**. Needless to say, the rate of convergence of the aperture field under the zero-thickness condition is much faster than that of the right-angled wedge condition, especially as the aperture is smaller.

3.2 Transmission properties

We next investigate the effect of the hole size and shape, screen thickness, and polarization on the transmission properties. Some results of the transmission coefficient are compared with those by other methods (Jin and Volakis [1], Brok and Urbach [7]). Unless otherwise noted, the following computations are made for $n_k = 6$. **Figure 9** shows the transmission coefficient T_E for square ($b/a = 1$) and rectangular ($b/a = 0.2$) holes less than the half-wavelength as a function of the normalized thickness d/a (in this case, all the waveguide modes become evanescent modes). It can be seen from the figure that the transmitted power rapidly decreases as the screen's thickness becomes large except for $ka = \pi/2 - 10^{-10}$, and this is due to the attenuation characteristic of the evanescent wave. However, rather strong transmission is observed for the elongated aperture ($b/a = 0.2$) when the value of d/a is small in spite of the fact that there is no propagating wave in the hole. This is considered to be closely related with the field singularity at long edges in addition to the small attenuation of the evanescent modes. By fitting asymptotic lines to T_E curves in **Figure 9** for the part where the value of d/a is large, we found an approximate expression for predicting the transmitted power, and it is given by

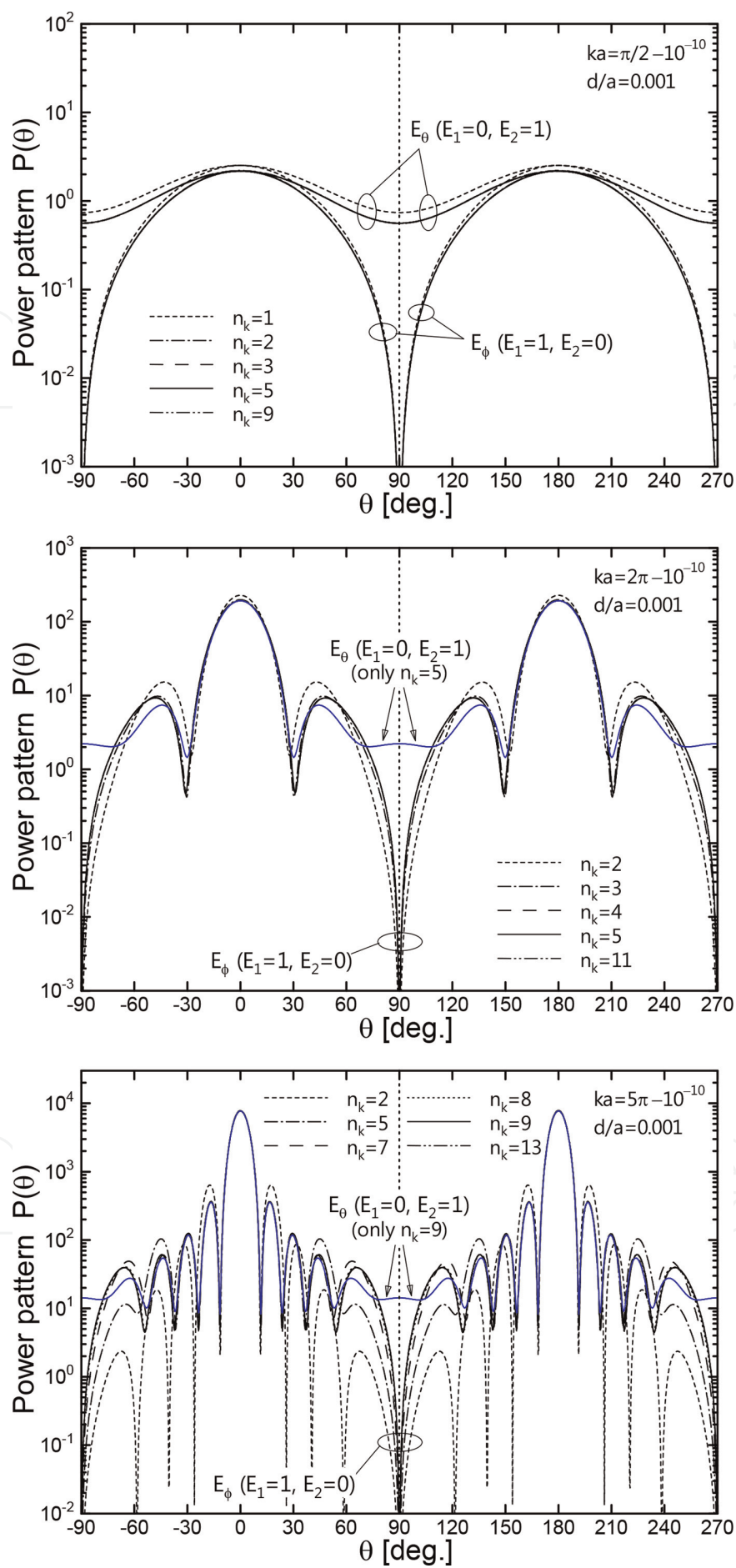


Figure 3.
 Power patterns of the far-fields diffracted by a square aperture ($a = b$) for $d/a = 0.001$ (thin screen case) in the $\phi = 0^\circ$ plane for the normal incidence ($\theta_o = \phi_o = 0^\circ$).

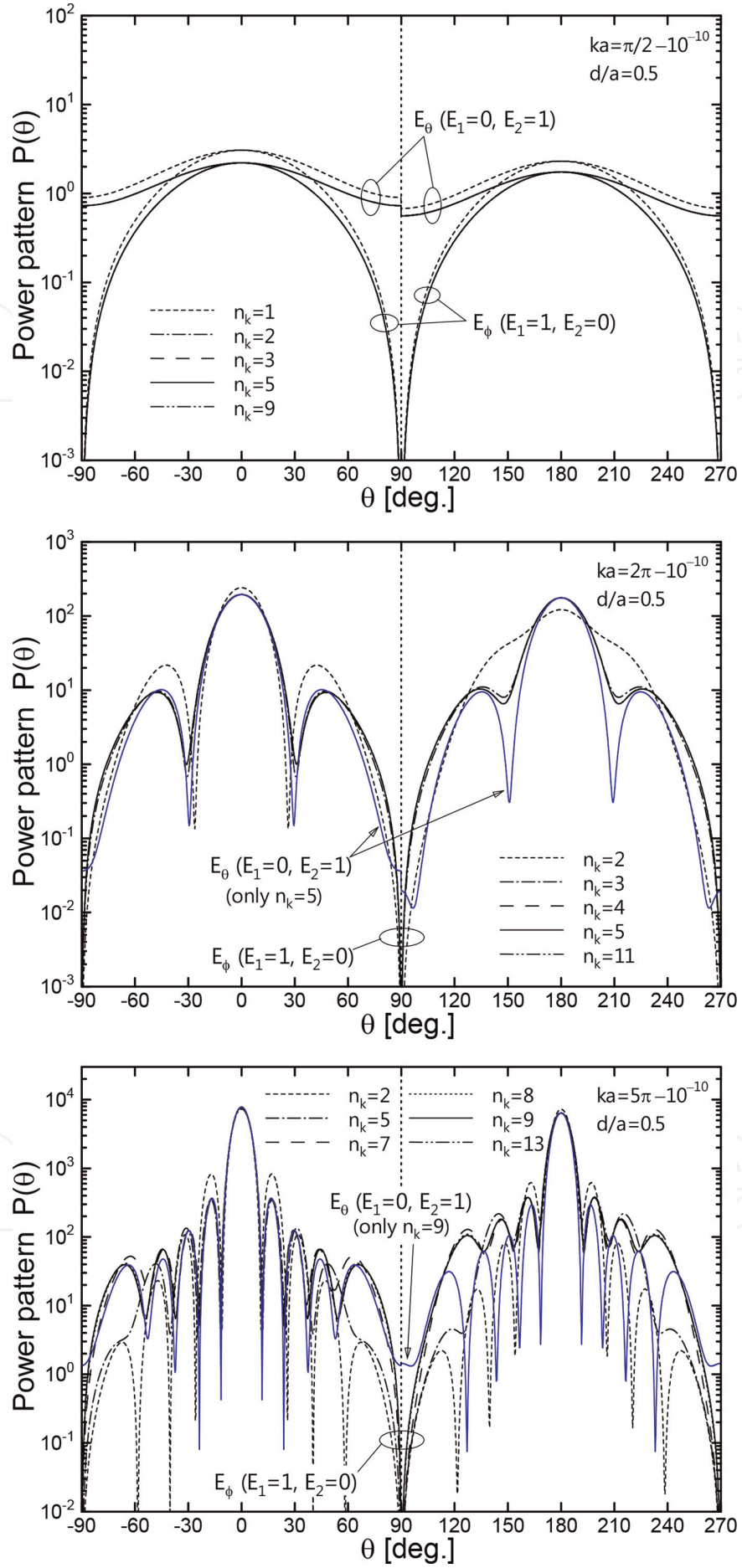


Figure 4. Power patterns of the far-fields diffracted by a square aperture ($a = b$) for $d/a = 0.5$ (thick screen case) in the $\phi = 0^\circ$ plane for the normal incidence ($\theta_o = \phi_o = 0^\circ$).

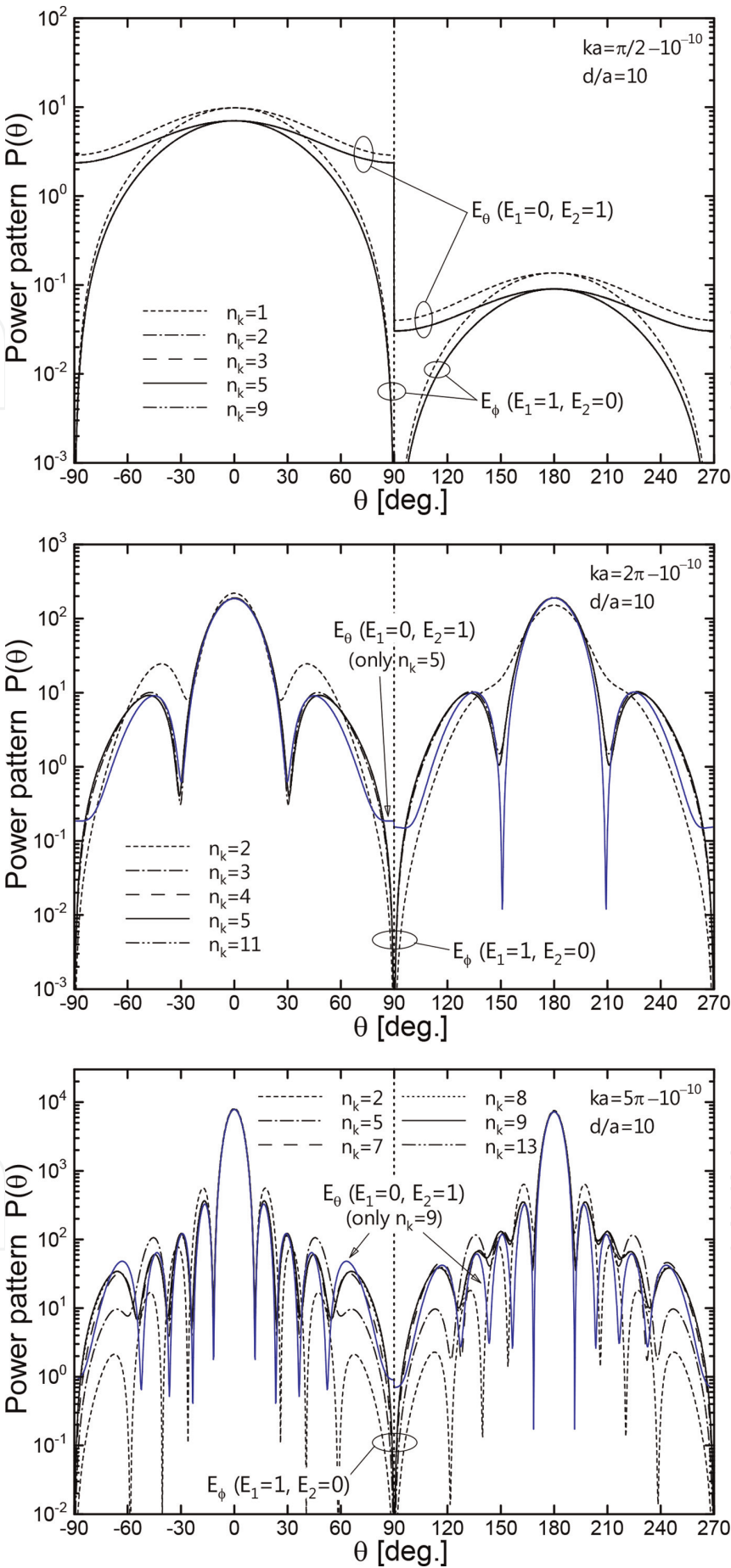


Figure 5. Power patterns of the far-fields diffracted by a square aperture ($a = b$) for $d/a = 10$ (deep hole case) in the $\phi = 0^\circ$ plane for the normal incidence ($\theta_o = \phi_o = 0^\circ$).

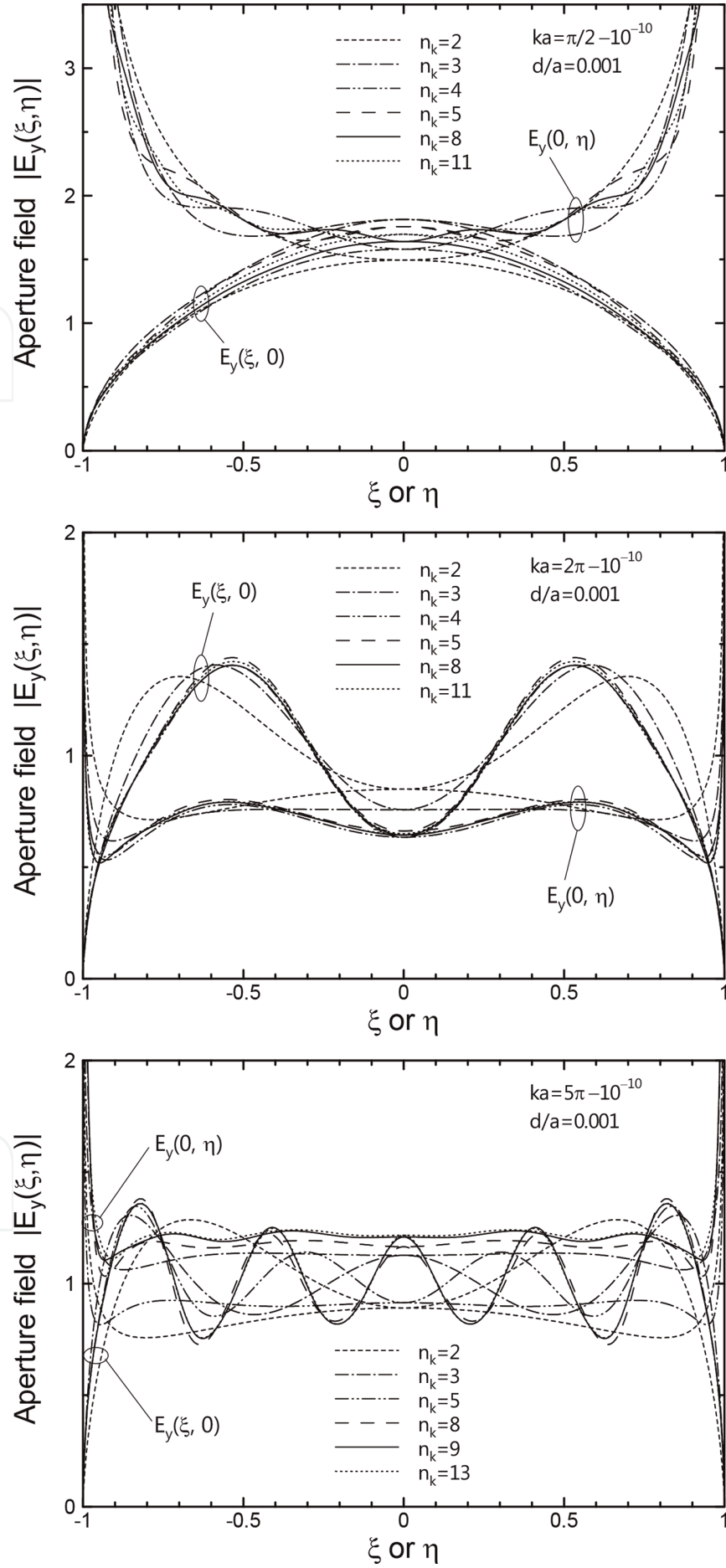


Figure 6. Amplitude distribution of the y-component of the aperture electric field $|E_y(\xi, \eta)|$ on the lower square aperture ($a/b = 1$, $z = -d$) for $d/a = 0.001$ (thin screen case) at $\theta_o = \phi_o = 0^\circ$ and E-polarized incidence.

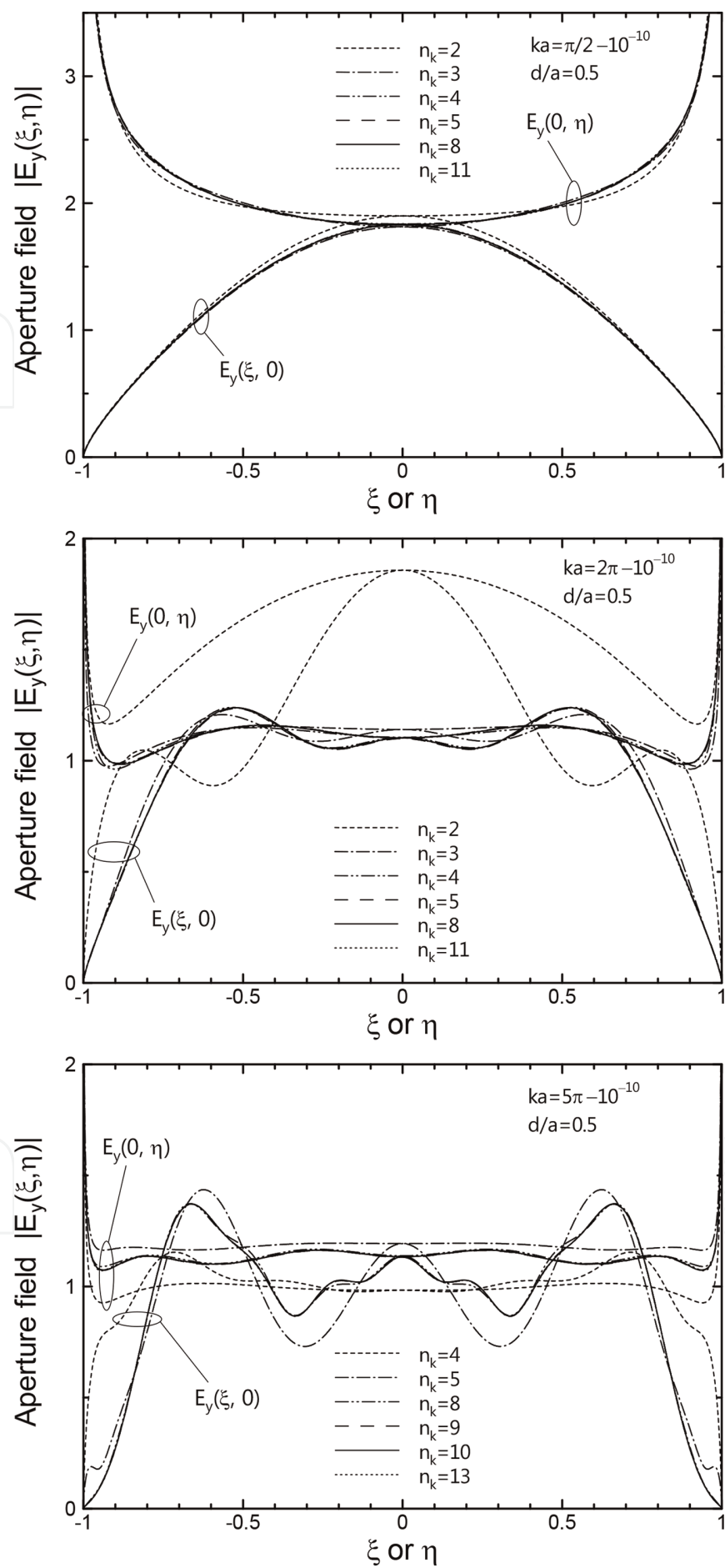


Figure 7.
Amplitude distribution of the y-component of the aperture electric field $|E_y(\xi, \eta)|$ on the lower square aperture ($a/b = 1$, $z = -d$) for $d/a = 0.5$ (thick screen case) at $\theta_o = \phi_o = 0^\circ$ and E-polarized incidence.

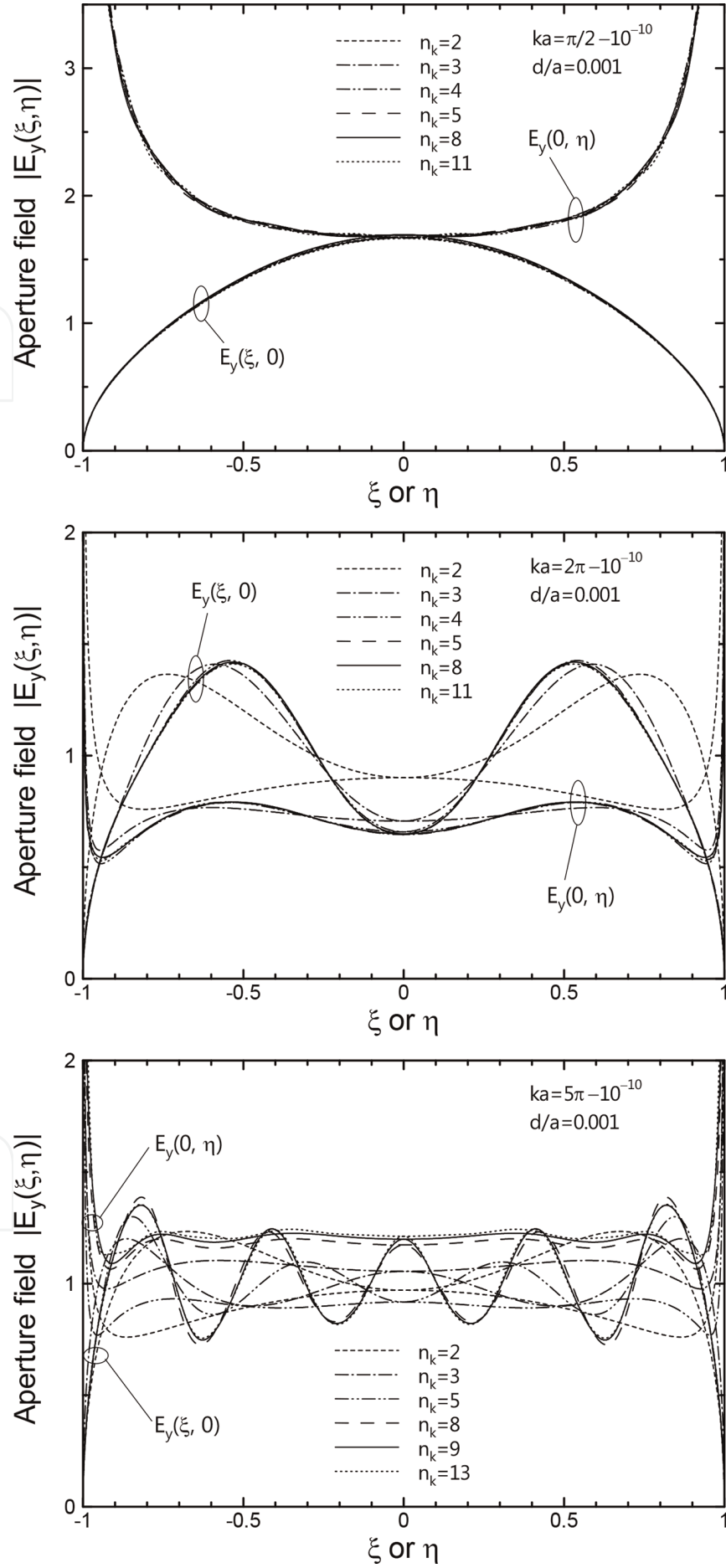


Figure 8. Amplitude distribution of the y-component of the aperture electric field $|E_y(\xi, \eta)|$ on the lower square aperture ($a/b = 1$, $z = -d$) for $d/a = 0.001$ (thin screen case) at $\theta_0 = \phi_0 = 0^\circ$ and E-polarized incidence. The edge condition of zero thickness screen ($\sigma = \tau' = 1$, $\tau = \sigma' = 0$) was used.

$$T_E = T_0 \exp \left(\frac{-2d}{a} \sqrt{\left(\frac{\pi}{2}\right)^2 - (ka)^2} \right) \tag{33}$$

where T_0 is a coefficient depending on ka and is shown in **Figure 10**.
The transmission coefficient is also calculated as a function of the normalized thickness d/a for various aperture sizes around the half-wavelength ($ka \approx \pi/2$), and the results are shown in **Figures 11** and **12** (our results completely agree with those by Brok and Urbach [7]). It can be seen from the figures that the T_E curves for apertures larger than the half-wavelength have oscillation, and this is due to the resonance of the

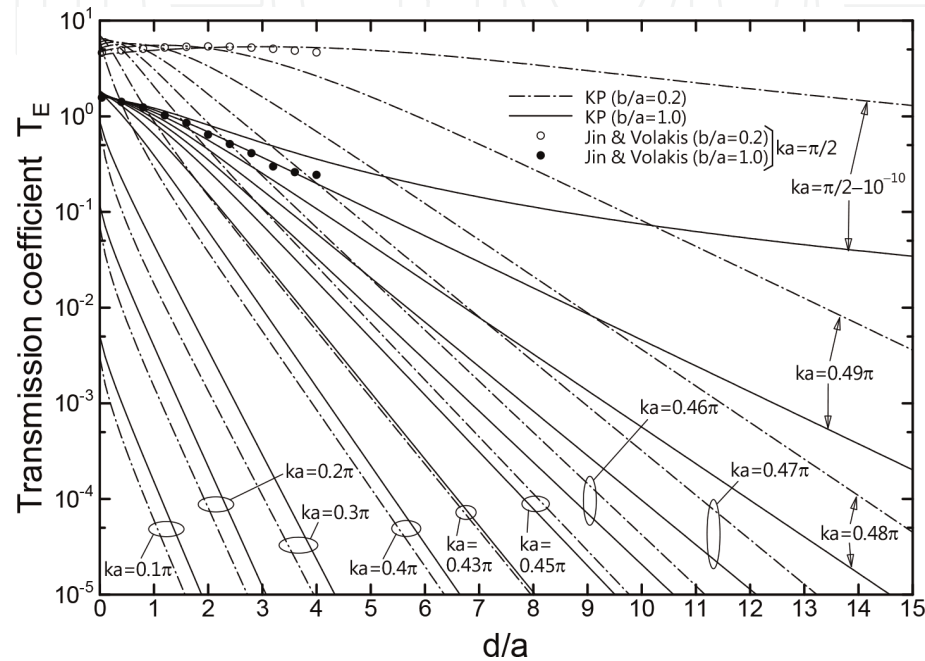


Figure 9.
 T_E as a function of the normalized screen thickness d/a for various ka values ($b/a = 1, 0.2$) at $\theta_o = \phi_o = 0^\circ$.

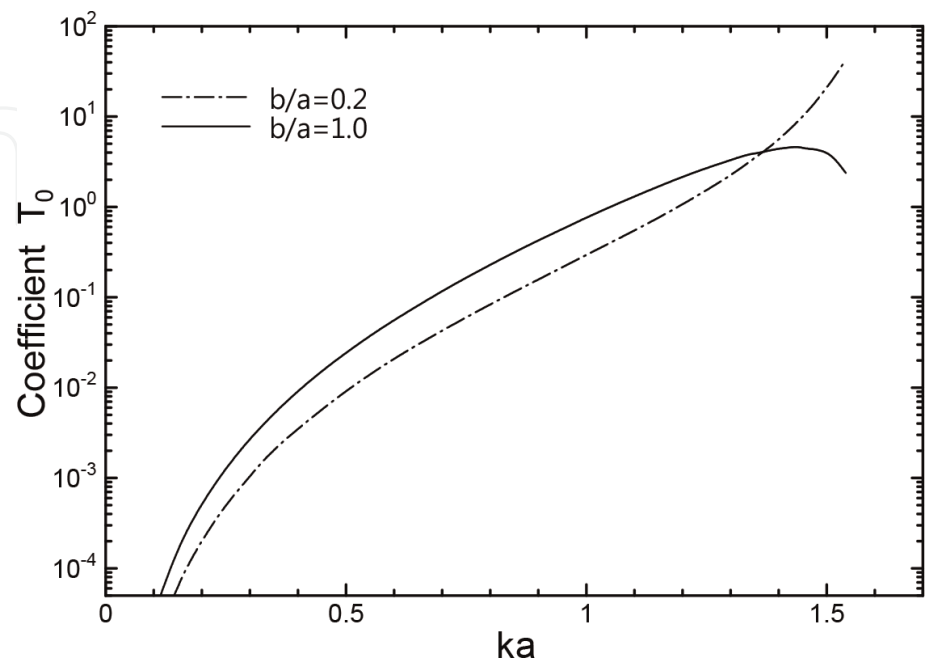
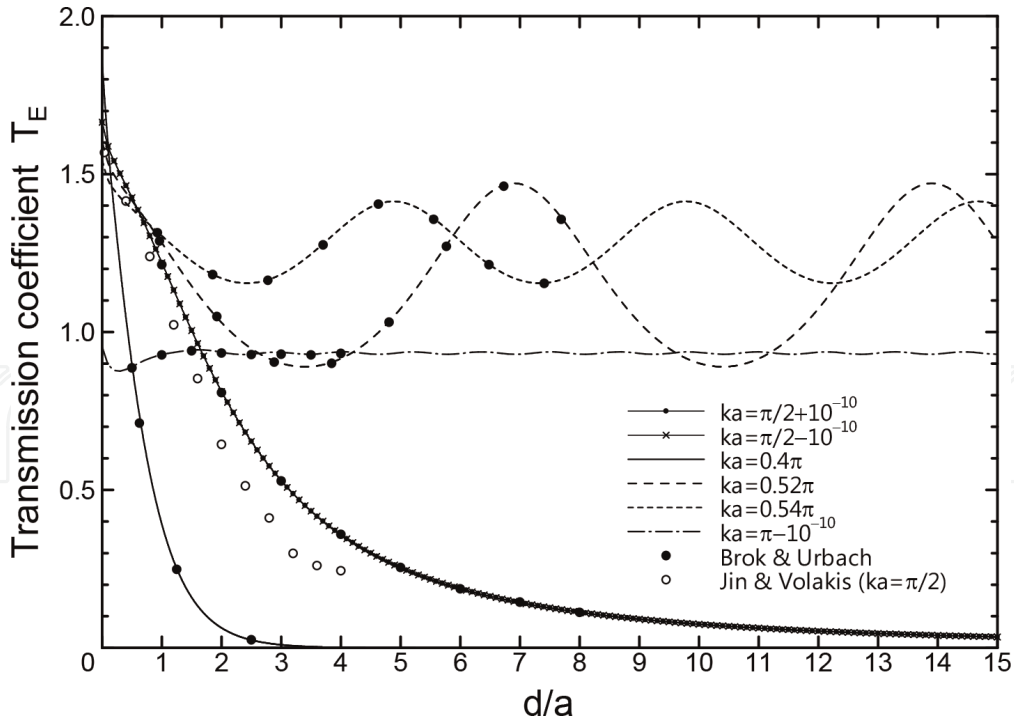


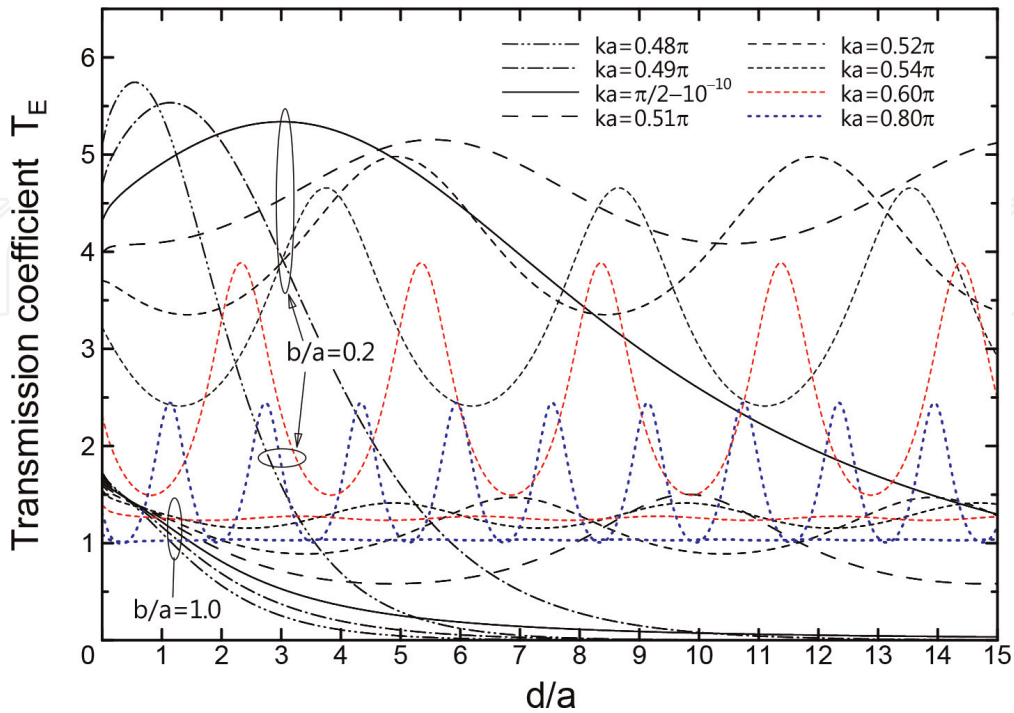
Figure 10.
Coefficient T_0 of asymptotic fitting lines for square ($b/a = 1$) and elongated rectangular ($b/a = 0.2$) apertures.


Figure 11.

T_E as a function of d/a for various ka values ($b/a = 1$) at $\theta_o = \phi_o = 0^\circ$ and E-polarized incidence.

propagating waveguide modes. The results of the total transmitted power normalized by $W_i(\theta_o = 0^\circ)$ are shown in **Figures 13** and **14** for various aperture sizes and shapes, and the curves of the transmitted power of the large aperture are complex (we think this is also due to the resonance of the waveguide modes).

Finally, we calculate the transmission coefficient T_E as functions of the normalized aperture length $2a/\lambda$ for a constant b value ($2b = 0.1\lambda$) and of the aspect ratio b/a for a constant hole area ($2a \times 2b = (\pi/4)^2$), and the results are given in


Figure 12.

Transmission coefficient T_E as a function of the normalized screen thickness d/a for various ka values ($b/a = 1, 0.2$) at $\theta_o = \phi_o = 0^\circ$ and E-polarized incidence.

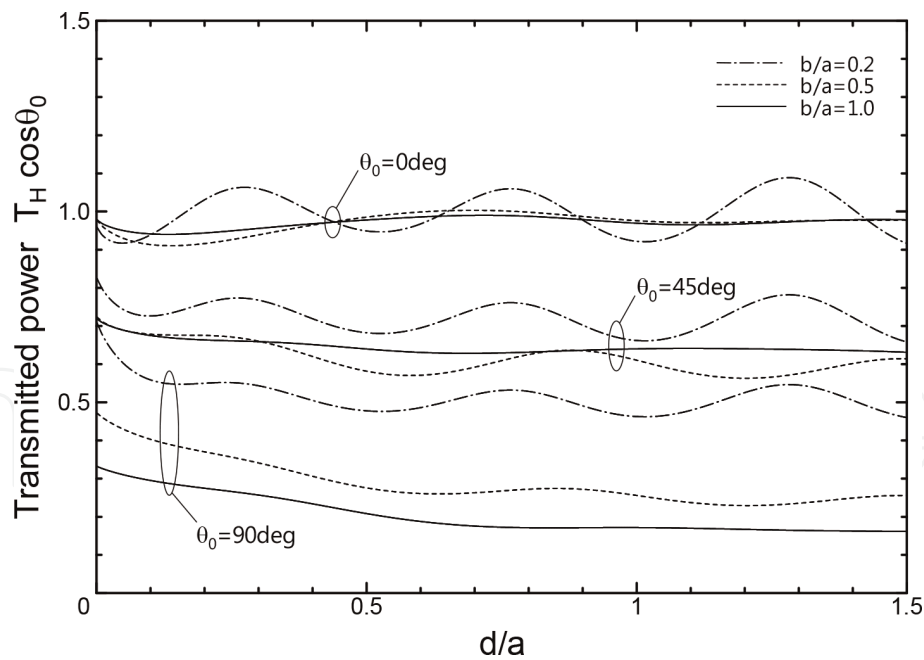


Figure 13.
Normalized transmitted power ($T_H \cos \theta_0$) through square and rectangular apertures ($ka = 2\pi - 10^{-10}$, $b/a = 1, 0.5, 0.2$) at $\theta_0 = 0^\circ, 45^\circ, 90^\circ$, and $\phi_0 = 90^\circ$.

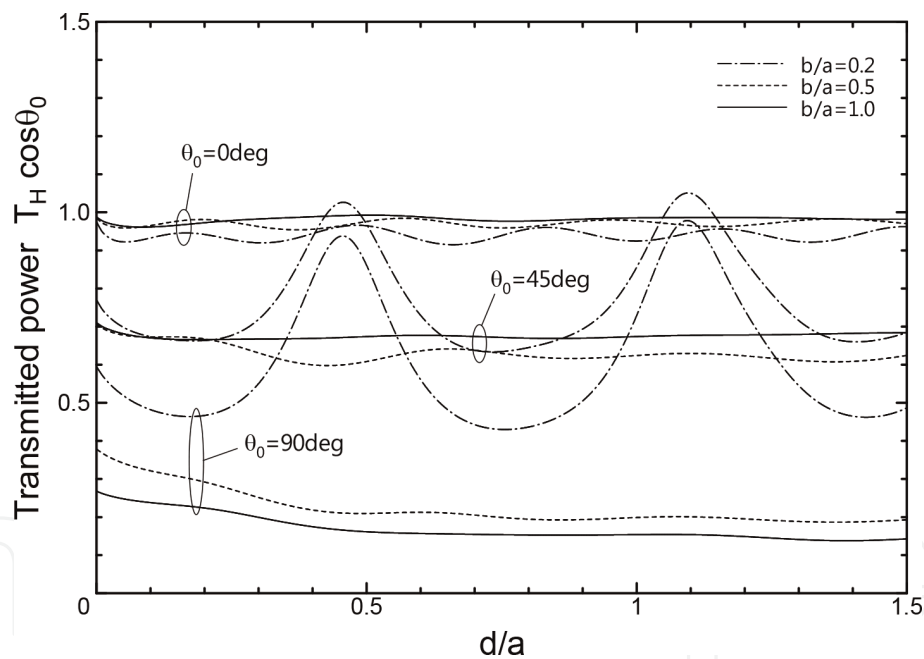
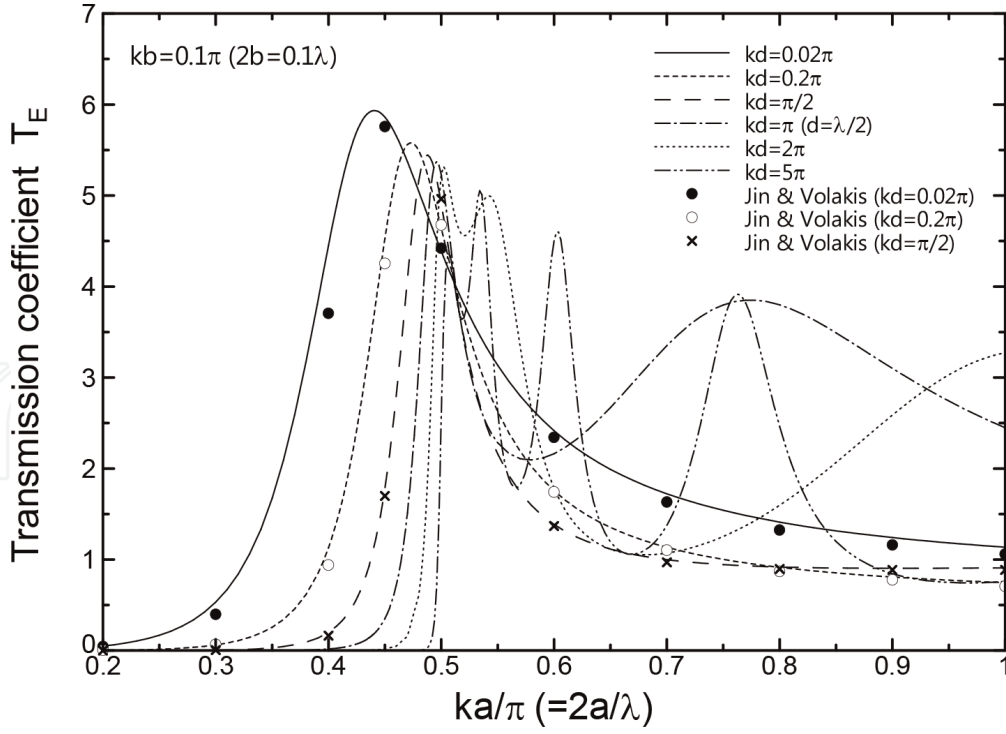
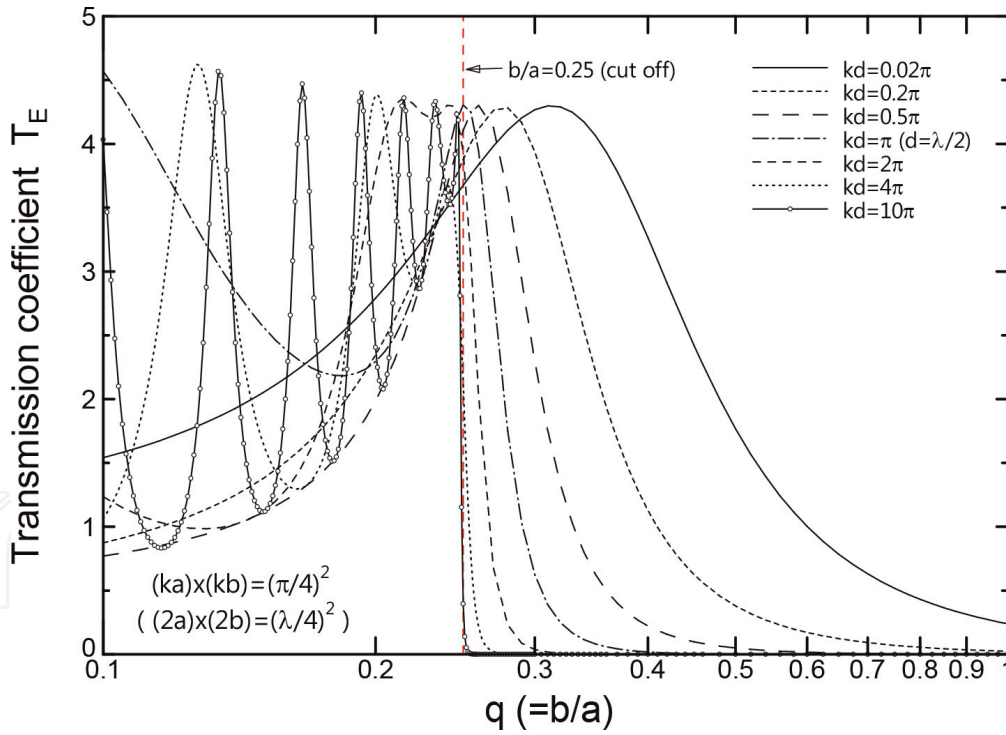


Figure 14.
Normalized transmitted power ($T_H \cos \theta_0$) through square and rectangular apertures ($ka = 3\pi - 10^{-10}$, $b/a = 1, 0.5, 0.2$) at $\theta_0 = 0^\circ, 45^\circ, 90^\circ$, and $\phi_0 = 90^\circ$.

Figures 15 and 16, respectively. In obtaining these results, the value of n_k was chosen to be 5. In **Figure 15**, all the waveguide modes for $ka < \pi/2$ become evanescent waves, but the strong power transmission is observed, and the position of the peak point approaches to $ka = \pi/2$ (cutoff frequency) as the screen thickness becomes large. For $ka > \pi/2$, we can find that the T_E curves have oscillations that are caused by the resonance of the lowest propagating mode in the waveguide. In **Figure 16**, $b/a = 0.25$ is a value related with the cutoff frequency, and all the waveguide modes become evanescent waves for $b/a > 0.25$. The similar situations of **Figure 15** can be also seen in this case.


Figure 15.

T_E as a function of the normalized aperture length ka/π with $kb = 0.1\pi$ for various kd values at $\theta_o = \phi_o = 0^\circ$.


Figure 16.

T_E as a function of the aspect ratio $q = b/a$ with the same area ($ka \times kb = (\pi/4)^2$) for various kd values at $\theta_o = \phi_o = 0^\circ$.

4. Conclusions

We have rigorously studied the diffraction of an electromagnetic plane wave by a rectangular hole in a perfectly conducting screen with a finite thickness by applying the KP method. The transmission coefficient, far-field pattern, and aperture electric field distribution were calculated to show the convergence of the solution.

The numerical results of the transmission coefficient were also presented as functions of the normalized thickness d/a to show the EM transmission property of the various sized holes. It was found from the results that the convergence of the KP solution is very rapid (for thin screen case, the edge condition of the zero-thickness plate is effective) and the transmitted power is strongly affected by the aperture size and shape, screen's thickness, incident angles, and polarization.

Acknowledgements


This work was partly supported by JSPS KAKENHI Grant Number 25390159 and 17K05150.

Author details

Hirohide Serizawa
National Institute of Technology, Numazu College, Numazu, Japan

*Address all correspondence to: serizawa@numazu-ct.ac.jp

IntechOpen

© 2019 The Author(s). Licensee IntechOpen. This chapter is distributed under the terms of the Creative Commons Attribution License (<http://creativecommons.org/licenses/by/3.0>), which permits unrestricted use, distribution, and reproduction in any medium, provided the original work is properly cited. 

References

- [1] Jin J-M, Volakis JL. Electromagnetic scattering by and transmission through a three-dimensional slot in a thick conducting plane. *IEEE Transactions on Antennas and Propagation*. 1991;**39**(4): 543-550. DOI: 10.1109/8.81469
- [2] Park HH, Eom HJ. Electromagnetic scattering from multiple rectangular apertures in a thick conducting screen. *IEEE Transactions on Antennas and Propagation*. 1999;**47**(6):1056-1060. DOI: 10.1109/8.777131
- [3] Stevanovic I, Mosig JR. Efficient electromagnetic analysis of line-fed aperture antennas in thick conducting screens. *IEEE Transactions on Antennas and Propagation*. 2004;**52**(11):2896-2903. DOI: 10.1109/TAP.2004.835268
- [4] Garcia-Vidal FJ, Martin-Moreno L, Ebbesen TW, Kuipers L. Light passing through subwavelength apertures. *Reviews of Modern Physics*. 2010;**82**(1): 729-787. DOI: 10.1103/RevModPhys.82.729
- [5] Garcia-Vidal FJ, Moreno E, Porto JA, Martin-Moreno L. Transmission of light through a single rectangular hole. *Physical Review Letters*. 2005;**95**(10): 103901. DOI: 10.1103/PhysRevLett.95.103901
- [6] Garcia-Vidal FJ, Martin-Moreno L, Moreno E, Kumar LKS, Gordon R. Transmission of light through a single rectangular hole in a real metal. *Physical Review B*. 2006;**74**(15):153411. DOI: 10.1103/PhysRevB.74.153411
- [7] Brok JM, Urbach HP. Extraordinary transmission through 1, 2 and 3 holes in a perfect conductor, modelled by a mode expansion technique. *Optics Express*. 2006;**14**(7):2552-2572. DOI: 10.1364/OE.14.002552
- [8] Meixner J. The behavior of electromagnetic fields at edges. *IEEE Transactions on Antennas and Propagation*. 1972;**AP-20**(4):442-446. DOI: 10.1109/TAP.1972.1140243
- [9] Hongo K, Serizawa H. Kobayashi potential in electromagnetism. *IEICE Transactions on Electronics*. 2012;**E95-C**(1):3-9. DOI: 10.1587/transele.E95.C.3
- [10] Hongo K, Sugaya H. Diffraction of an acoustic plane wave by a rectangular plate. *Journal of Applied Physics*. 1997;**82**(6):2719-2729. DOI: 10.1063/1.366266
- [11] Hongo K, Serizawa H. Diffraction of electromagnetic plane wave by a rectangular plate and a rectangular hole in the conducting plate. *IEEE Transactions on Antennas and Propagation*. 1999;**47**(6):1029-1041. DOI: 10.1109/8.777128
- [12] Hongo K, Serizawa H. Diffraction of an acoustic plane wave by a rectangular hole in an infinitely large rigid screen. *The Journal of the Acoustical Society of America*. 1999;**106**(1):29-35. DOI: 10.1121/1.427033
- [13] Serizawa H, Hongo K. Evaluation of an acoustic plane wave transmitted through a rectangular hole in a thick hard screen. *Wave Motion*. 2002;**36**(2): 103-117. DOI: 10.1016/S0165-2125(01)00116-0
- [14] Serizawa H, Hongo K. Radiation from a flanged rectangular waveguide. *IEEE Transactions on Antennas and Propagation*. 2005;**53**(12):3953-3962. DOI: 10.1109/TAP.2005.859748
- [15] Serizawa H, Hongo K. Transmission through a rectangular hole in a thick conducting screen. *IEICE Technical Report (AP)*. 2009;**109**(218):31-36
- [16] Serizawa H. Diffraction of a plane wave by a rectangular hole in a thick conducting screen. In: *Proceedings of*

the 9th European Conference on
Antennas and Propagation (EuCAP
2015), MA12 EMTheory. Lisbon: IEEE;
2015

[17] Serizawa H. Plane wave diffraction
by a small rectangular aperture in a
thick conducting screen. In: Proceedings
of the 2016 International Conference on
Electromagnetics in Advanced
Applications (ICEAA '16). Cairns:
IEEE; 2016. pp. 890-893. DOI: 10.1109/
ICEAA.2016.7731545

[18] Serizawa H. Plane wave diffraction
by a large rectangular aperture in a thick
conducting screen. In: Proceedings of
the 2017 International Conference on
Electromagnetics in Advanced
Applications (ICEAA '17). Verona:
IEEE; 2017. pp. 1612-1615. DOI:
10.1109/ICEAA.2017.8065597